

Interacting Particle Systems for Fast Linear Quadratic RL

Anant A. Joshi

University of Illinois Urbana-Champaign

ANANTAJ2@ILLINOIS.EDU

Heng-Sheng Chang

University of Illinois Urbana-Champaign

HSCHANG2@ILLINOIS.EDU

Amirhossein Taghvaei

University of Washington Seattle

AMIRTAG@UW.EDU

Prashant G. Mehta

University of Illinois Urbana-Champaign

MEHTAPG@ILLINOIS.EDU

Sean P. Meyn

University of Florida at Gainesville

MEYN@ECE.UFL.EDU

Abstract

This paper is concerned with the design of algorithms based on systems of interacting particles to represent, approximate, and learn the optimal control law for reinforcement learning (RL). The primary contribution is that convergence rates are greatly accelerated by the interactions between particles. Theory focuses on the linear quadratic stochastic optimal control problem for which a complete and novel theory is presented. Apart from the new algorithm, sample complexity bounds are obtained, and it is shown that the mean square error scales as $1/N$ where N is the number of particles. The theoretical results and algorithms are illustrated with numerical experiments and comparisons with other recent approaches, where the faster convergence of the proposed algorithm is numerically demonstrated.

Keywords: List of keywords

1. Introduction

This paper concerns approaches to reinforcement learning (RL) based on the construction of interacting particle systems. The development is in continuous time, and the state is assumed to evolve according to a linear stochastic differential equation (SDE),

$$dX_t = (AX_t + BU_t)dt + \sigma dW_t, \quad X_0 = x \quad (1)$$

where $X := \{X_t : 0 \leq t \leq T\}$ is the \mathbb{R}^d -valued state process, $U := \{U_t : 0 \leq t \leq T\}$ is the \mathbb{R}^m -valued control input, and $W := \{W_t : 0 \leq t \leq T\}$ is a standard Brownian motion (B.M.), and A, B, σ are matrices of appropriate dimensions.

The proposed approach is related to actor-only methods, also known as the policy optimization (PO) approach, of which Williams' REINFORCE algorithm is most classical [Williams \(1992\)](#). The linear model is the subject of recent work in PO: two types of optimal control objectives have been considered, namely, linear quadratic Gaussian (LQG) ([Basei et al., 2022](#)) linear exponential quadratic Gaussian (LEQG) ([Zhang et al., 2021b](#); [Roulet et al., 2020](#)), and average cost versions of these ([Krauth et al., 2019](#); [Abbasi-Yadkori et al., 2019](#); [Yang et al., 2019](#); [Cassel and Koren, 2021](#); [Yaghmaie et al., 2023](#); [Hernández-Hernández and Salazar-Sánchez, 2023](#)).

A standard PO approach in the linear quadratic setting is special because the policies $\{\kappa^\theta : \theta \in \mathbb{R}^n\}$ may be chosen deterministic and linear. A basic algorithm is described as the following recursion: Starting from an initial stabilizing gain K^0 , a sequence of gains $\{K^j : j = 1, 2, \dots, M\}$ are learnt. During the j -th iteration, the gain K^j is evaluated by simulating N copies of the model over a time-horizon:

$$dX_t^i = (AX_t^i + BK_t^j X_t^i)dt + \sigma dW_t^i, \quad 0 \leq t \leq T, \quad 1 \leq i \leq N \quad (2a)$$

$$X_0^i \stackrel{\text{i.i.d.}}{\sim} \mathcal{N}(0, I), \quad 1 \leq i \leq N \quad (2b)$$

These evaluations are helpful to compute the gain K^{j+1} through a gradient-descent procedure.

When $N = 1$ the algorithm might be applied using observed samples from a physical system; otherwise, this technique requires a simulator to generate particles. The main message of this paper is that the use of a simulator combined with carefully designed mean-field interactions between simulations (the particles) will ensure far greater efficiency in the learning process.

Algorithm proposed in this paper. Simulate an interacting particle system:

$$dY_t^i = \underbrace{AY_t^i dt + Bd\eta_t^i + \sigma dW_t^i}_{\text{copy of model}} + \underbrace{\mathcal{A}_t(Y_t^i; p_t^{(N)})dt}_{\text{mean-field interaction}}, \quad 0 \leq t \leq T, \quad 1 \leq i \leq N \quad (3a)$$

$$Y_T^i \stackrel{\text{i.i.d.}}{\sim} \mathcal{N}(0, \mathcal{Y}), \quad 1 \leq i \leq N, \quad (3b)$$

where $p_t^{(N)}$ is the empirical distribution of the ensemble $\{Y_t^i : 1 \leq i \leq N\}$. The specification of the terminal condition at time $t = T$ means that the system is simulated backward-in-time. The three design variables are as follows:

- (i) \mathcal{Y} is the covariance matrix to sample the N particles at the terminal time.
- (ii) $\eta := \{\eta^i : 1 \leq i \leq N\}$ where $\eta^i := \{\eta_t^i, : 0 \leq t \leq T\}$ is the control input for the i -th particle. These inputs are designed to be independent B.M. with a prescribed covariance.
- (iii) $\mathcal{A} := \{\mathcal{A}_t : 0 \leq t \leq T\}$ is a mean-field process which couples the simulations. The phrase “mean-field” means that the coupling depends *only* upon the (empirical) distribution $p_t^{(N)}$.

The triple $(\mathcal{Y}, \eta, \mathcal{A})$ are designed with the goal that the empirical covariance of the ensemble $\{Y_t^i : 1 \leq i \leq N\}$ approximates the solution of the differential Riccati equation (DRE) at time t . The resulting system is referred to as the *dual ensemble Kalman filter*.

Contributions: The paper builds on [Joshi et al. \(2022\)](#) to include stochastic control systems. The novel aspects of the present paper are three-fold: **(i)** the algorithms and the analysis are extended to stochastic and robust/risk sensitive settings of the problem in a single unified framework; **(ii)** an error analysis is provided for finite but large N interacting particle system; and **(iii)** sample complexity results are obtained and comparison of the same provided against state-of-the-art algorithms for linear quadratic RL (iv) comparisons are presented to the path integral control framework, which is related to our approach and used widely in RL and robotics. (v) This paper includes numerical simulation and comparison for two benchmark example problems from previous works in this area.

The salient features of the proposed algorithm are as follows: **(i)** It is not necessary that the matrix A is Hurwitz or that a stabilizing gain matrix K^0 is known (this is an assumption in many

Table 1: Expressions for DRE, where $D := BR^{-1}B^T$ and $\Sigma := \sigma\sigma^T$.

| Cost | $\mathcal{D}(\Lambda)$ | $\mathcal{D}^\dagger(\Lambda)$ |
|------|--|---|
| LQG | $A^T\Lambda + \Lambda A + C^TC - \Lambda D\Lambda$ | $A\Lambda + \Lambda A^T - D + \Lambda C^TC\Lambda$ |
| LEQG | $A^T\Lambda + \Lambda A + C^TC - \Lambda(D - \theta\Sigma)\Lambda$ | $A\Lambda + \Lambda A^T - \frac{1}{ \theta }(D - \theta\Sigma) + \theta \Lambda C^TC\Lambda$ |

of the prior studies on PO); and **(ii)** convergence theory relies on law of large numbers (LLN) and spectral constant known from the DRE theory. Specifically, as $N \rightarrow \infty$, the proposed algorithm yields a learning rate that approximates the exponential rate of convergence of the solution of the DRE; and **(iii)** it alleviates issues like weight collapse and curse of dimensionality that are inherited by algorithms based on the importance sampling paradigm.

2. Problem formulation

Notation: $\|\cdot\|_F$ denotes Frobenius norm for matrices, $|\cdot|$ denotes 2-norm for vectors and $|\cdot|_M$ denotes weighted 2-norm under positive definite matrix M , that is, $|z|_M := z^T M z$, $\mathcal{N}(\text{mean}, \text{covariance})$ denotes normal distribution, \mathbb{I} is used for identity matrix.

In linear quadratic settings, the cost function is quadratic as follows:

$$c(x, a) = \frac{1}{2}|Cx|^2 + \frac{1}{2}|a|_R^2, \quad x \in \mathbb{R}^d, \quad a \in \mathbb{R}^m$$

Based on this, the following types of stochastic optimal control problems, linear quadratic Gaussian (LQG), linear exponential quadratic Gaussian (LEQG), and their average counterparts are considered (with $\theta \in \mathbb{R} \setminus \{0\}$):

$$J_T^{\text{LQG}}(U) := \mathbb{E} \left[\int_0^T c(X_t, U_t) dt + \frac{1}{2} |X_T|_G^2 \right], \quad (\text{LQG})$$

$$J_T^{\text{LEQG}}(U) := \theta^{-1} \log \mathbb{E} \left[\exp \theta \left\{ \int_0^T c(X_t, U_t) dt + \frac{1}{2} |X_T|_G^2 \right\} \right], \quad (\text{LEQG})$$

$$J^{\text{AVG}, i}(U) := \limsup_{T \rightarrow \infty} \frac{1}{T} J_T^i(U), \quad i \in \{\text{LQG}, \text{LEQG}\}. \quad (\text{AVG})$$

For the LEQG problem, θ is referred to as the risk parameter: The case $\theta > 0$ is known as risk-averse and $\theta < 0$ as risk-seeking Nagai (2013). The problem is to choose the control U to minimize the respective value $J(U)$ subject to the linear Gaussian dynamics (1). A standard set of assumptions—that are also made here—are now listed.

Assumption 1 (A, B) is controllable, and $C^TC, R, G \succ 0$ and for LEQG, $BR^{-1}B^T - \theta\sigma\sigma^T \succ 0$.

The main point of difference from the classical treatment is that the linear Gaussian model (1) is available *only* in the form of a simulator.

Definition 1 (Simulator) A simulator of (1), denoted \mathcal{S} , takes the current state $x \in \mathbb{R}^d$, control $a \in \mathbb{R}^m$ and (small) time-step τ as input and gives the following random variable as output

$$\mathcal{S}(x, a; \tau) = (Ax + Ba)\tau + \sigma\Delta W \quad \text{where } \Delta W \stackrel{i.i.d.}{\sim} \mathcal{N}(0, \mathbb{I}\tau).$$

Remark 2 (Simulations and RL) *The simulator takes the current state and control at every call, and the random variables ΔW are i.i.d. from $\mathcal{N}(0, \tau)$ for every simulator call. A standard assumption in RL is that the state is available at every time t . Outside of a simulation type setting, it is difficult to describe a system where such an assumption holds: Most real-world systems have partial observation of the states through noisy sensor outputs. Next, many types of RL algorithms implement multiple iterations of the type (2), e.g., (Krauth et al., 2019, Algorithm 1,2), (Yang et al., 2019, Algorithm 2), (Basei et al., 2022, Algorithm 1), (Cassel and Koren, 2021, Algorithm 1) (Yaghmaie et al., 2023, Algorithm 3), (Zhang et al., 2021b, Algorithm 2), (Cui et al., 2023, Algorithm 2), (Lai and Xiong, 2024, Algorithm 1). More discussion in Appendix A.*

2.1. Riccati equation and the Q function

Consider a matrix-valued process $\{P_t : 0 \leq t \leq T\}$ obtained from solving the DRE as follows:

$$-\frac{d}{dt}P_t = \mathcal{D}(P_t), \quad 0 \leq t \leq T, \quad P_T = G \quad (4)$$

where the expressions for the Riccati operator $\mathcal{D}(\cdot)$ are given in Table 1. While the DRE is the optimality equation for the finite time-horizon, the average cost solution is obtained by letting the time-horizon $T \rightarrow \infty$. Because (A, B) is controllable and (A, C) is observable, for any fixed time t , $P_t \rightarrow \bar{P}$ which solves the ARE: $\mathcal{D}(\bar{P}) = 0$ ((Kwakernaak and Sivan, 1972, Theorem 3.7)).

Definition 3 (Q-function) *The continuous-time Q-function (or Hamiltonian) is defined as*

$$\begin{aligned} Q(x, a; t) &:= c(x, a) + x^\top P_t (Ax + Ba), \quad 0 \leq t \leq T, \quad x \in \mathbb{R}^d, \quad a \in \mathbb{R}^m && \text{for LQG, LEQG} \\ \bar{Q}(x, a) &:= c(x, a) + x^\top \bar{P} (Ax + Ba), \quad x \in \mathbb{R}^d, \quad a \in \mathbb{R}^m && \text{for AVG} \end{aligned}$$

Then (see Liberzon (2012)),

$$U_t^{\text{opt}} = \begin{cases} \arg \min_{a \in \mathbb{R}^m} Q(X_t, a; t), & 0 \leq t \leq T, \quad \text{LQG, LEQG} \\ \arg \min_{a \in \mathbb{R}^m} \bar{Q}(X_t, a), & \text{AVG} \end{cases}$$

Because the Q function is quadratic, it is easily verified that the optimal control law is linear:

$$U_t^{\text{opt}} = \begin{cases} K_t X_t, & K_t := -R^{-1} B^\top P_t, \quad 0 \leq t \leq T, \quad \text{LQG, LEQG} \\ \bar{K} X_t, & \bar{K} := -R^{-1} B^\top \bar{P}, \quad \text{AVG} \end{cases}$$

The analysis of this paper requires consideration of P_t^{-1} . Since $G \succ 0$, it holds that $P_t \succ 0$ for $0 \leq t \leq T$ (Brockett, 2015, Sec. 24). Therefore, P_t^{-1} is well-defined. For every $t \in [0, T]$,

$$S_t := P_t^{-1} \text{ for LQG;} \quad \text{and} \quad S_t := (|\theta|P_t)^{-1} \text{ for LEQG.} \quad (5)$$

Then $\{S_t : 0 \leq t \leq T\}$ solves the dual DRE as follows:

$$-\frac{d}{dt}S_t = \mathcal{D}^\dagger(S_t), \quad 0 \leq t \leq T, \quad S_T = G^{-1}$$

3. Interacting particle algorithm

In this section, two sets of algorithms are described to approximate the optimal control law based only on the use of the simulator. These are as follows:

- **Offline algorithm for solving DRE.** The goal is to learn an approximation of the Q-function. These approximations for the finite time-horizon and the average cost problems are denoted as $\mathcal{Q}^{(N)}$ and $\bar{\mathcal{Q}}^{(N)}$, respectively. Additional background and justification appears in Appendix A.

- **Online algorithm for computing the optimal control.** For each fixed time t , the optimal control is obtained by taking an arg min of approximate Q-function.

3.1. Dual EnKF for approximating solution of DRE

Consider the interacting particle system (3). The triple $(\mathcal{Y}, \eta, \mathcal{A})$ is designed as follows:

(i) **Design of Y_T^i :** Sample $Y_T^i \stackrel{\text{i.i.d.}}{\sim} \mathcal{N}(0, S_T)$ for $i = 1, 2, \dots, N$.

(ii) **Design of η^i :** The input η^i are i.i.d copies of a B.M. η whose covariance is

$$\text{Cov}(\eta) = R^{-1} \text{ for LQG, and } \text{Cov}(\eta) = (\sqrt{|\theta|}R)^{-1} \text{ for LEQG.} \quad (6)$$

In the context of RL, η has an interpretation as the exploration signal. The form (6) of the covariance means that the cheaper control directions are explored more.

(iii) **Design of \mathcal{A}_t :** The interaction term is a mean-field type linear control law as follows:

$$\mathcal{A}_t(z; p_t^{(N)}) := \begin{cases} \frac{1}{2}L_t^{(N)}C(z + n_t^{(N)}) + \frac{1}{2}\Sigma(S_t^{(N)})^{-1}(z - n_t^{(N)}); & \text{LQG} \\ \frac{|\theta|}{2}L_t^{(N)}C(z + n_t^{(N)}) + \text{sgn}(\theta)\Sigma(S_t^{(N)})^{-1}(z - n_t^{(N)}); & \text{LEQG} \end{cases} \quad (7)$$

where $\Sigma := \sigma\sigma^\top$, $n_t^{(N)} := N^{-1} \sum_i Y_t^i$, and

$$L_t^{(N)} := \frac{1}{N-1} \sum_{i=1}^N (Y_t^i - n_t^{(N)})(CY_t^i - Cn_t^{(N)})^\top, \quad S_t^{(N)} := \frac{1}{N-1} \sum_{i=1}^N (Y_t^i - n_t^{(N)})(Y_t^i - n_t^{(N)})^\top.$$

From (5), provided the right-hand side is well-defined,

$$P_t^{(N)} := (S_t^{(N)})^{-1} \text{ for LQG, and } P_t^{(N)} := (|\theta|S_t^{(N)})^{-1}; \text{ for LEQG,} \quad (8)$$

and for the average cost problem, $\bar{P}^{(N)} := P_0^{(N)}$. The error analysis is the subject of the following main result of this paper.

Theorem 4 Consider the dual EnKF (3) under Assumption 1. Then for $N \geq d + 1$, for each fixed t ,

$$\text{(Finite-horizon)} \quad \mathbb{E}[\|S_t^{(N)} - S_t\|_F^2] \leq \frac{C_1}{N}, \quad \mathbb{E}[\|P_t^{(N)} - P_t\|_F^2] \leq \frac{C_4}{N}, \quad 0 \leq t \leq T, \quad (9a)$$

$$\text{(Average cost)} \quad \mathbb{E}[\|S_t^{(N)} - \bar{S}\|_F^2] \leq \frac{C_2}{N}, \quad \mathbb{E}[\|P_t^{(N)} - \bar{P}\|_F^2] \leq \frac{C_5}{N}, \quad \text{as } T \rightarrow \infty \quad (9b)$$

(where C_1, C_2, C_3, C_4 are model dependent but time-independent constants). For the average cost problem, there exists a constant $\lambda > 0$ such that exponential convergence to the stationary solution is obtained as follows:

$$\mathbb{E}[\|S_t^{(N)} - \bar{S}\|_F^2] \leq \frac{C_2}{N} + C_3 e^{-2\lambda(T-t)} \mathbb{E}[\|S_T^{(N)} - \bar{S}\|_F^2], \quad 0 \leq t \leq T \quad (10)$$

Proof These bounds are based on [Bishop and Moral \(2019\)](#). The proof appears in [Appendix C.1](#). ■

Formula (10) is important because λ is the rate for learning the optimal solution. The constant λ is the spectral constant related to the exponential convergence of the solution of the DRE to the solution of the ARE ([Kwakernaak and Sivan, 1972](#)). As seen in the proof, the interaction term \mathcal{A} is responsible for this property. The formula is useful to see the relation between the simulation horizon T and the error. For $\varepsilon > 0$, let $t = 0$ in (10), $N > O(\frac{1}{\varepsilon^2})$ and $T > O(\log(\frac{1}{\varepsilon}))$, then error is smaller than ε . The offline dual EnKF algorithm (Algorithm 1 in [Appendix B](#)) presents a method to simulate the interacting particle system (3) using only access to a simulator. For the numerical approximation of the SDE, a first order Euler-Maruyama method is used and may be replaced with a higher order method.

3.2. Algorithm for approximating optimal control

If the matrix B is available, then the optimal control input at time t is approximated as follows:

$$U_t^{(N)} = \begin{cases} K_t^{(N)} X_t, & K_t^{(N)} := -R^{-1} B^T P_t^{(N)}, & 0 \leq t \leq T, & \text{LQG, LEQG} \\ \bar{K}^{(N)} X_t, & \bar{K}^{(N)} := -R^{-1} B^T \bar{P}^{(N)}, & & \text{AVG} \end{cases}$$

For the case where an explicit form of B is not known, then the simulator is used to obtain an empirical approximation of the Q-function as follows:

Definition 5 (Empirical Q-function) *The empirical approximations are defined as*

$$\begin{aligned} \mathcal{Q}^{(N)}(x, a; t, \tau) &:= c(x, a)\tau + x^T P_t^{(N)} \mathcal{S}(x, a; \tau), & 0 \leq t \leq T, & x \in \mathbb{R}^d, a \in \mathbb{R}^m & (11) \\ \bar{\mathcal{Q}}^{(N)}(x, a; \tau) &:= c(x, a)\tau + x^T \bar{P}^{(N)} \mathcal{S}(x, a; \tau), & x \in \mathbb{R}^d, a \in \mathbb{R}^m & \end{aligned}$$

Based on the empirical Q-function, the optimal control is given by

$$U_t^{(N)} \tau = \begin{cases} \arg \min_{a \in \mathbb{R}^m} \mathbb{E} [\mathcal{Q}^{(N)}(X_t, a; t, \tau) | X_t], & 0 \leq t \leq T, & \text{LQG, LEQG} \\ \arg \min_{a \in \mathbb{R}^m} \mathbb{E} [\bar{\mathcal{Q}}(X_t, a; \tau) | X_t], & & \text{AVG} \end{cases}$$

The expectation on the right-hand side is necessary because the simulator is noisy. A most straightforward implementation is to simply replace the expectation with a single sample—as one does in a stochastic gradient descent procedure. With additional computational budget, the expectation is approximated through N_e evaluations in a batch.

To evaluate the arg min, one may use a zero order optimization framework ([Bach and Perchet, 2016](#)). A simpler algorithm is obtained by noting that, like the Q function, the empirical Q function is also a quadratic function of the state, of the form $\frac{1}{2} a^T R a + B^T a + \varphi(x)$ where $\varphi(\cdot)$ is now a random function. For the case when the number of control inputs m is small, optimal control is approximated by evaluating the Q function for $a = R^{-1} e_i$ where $\{e_1, e_2, \dots, e_m\}$ are basis vectors in \mathbb{R}^m . Details of the procedure appear in [Appendix C.3](#) where the resulting empirical approximation of the optimal gain is described and the following bound is shown:

$$\mathbb{E}[\|\hat{K}_t^{(N)} - K_t\|_F^2] \leq \frac{C_6}{N} + \frac{nC_7}{N_e \tau}, \quad 0 \leq t \leq T \quad (12)$$

Table 2: Complexity bounds in terms of error ε . These estimates are reported for the error in approximating gain in (Zhang et al., 2021b, Theorem 4.3) and (Krauth et al., 2019, Theorem 2.2); and the error in approximating the optimal cost in (Cassel and Koren, 2021, Lemma 6) and (Yang et al., 2019, Theorem 4.3).

| Algorithm | particles/samples | simulation time | iterations |
|-------------------------|------------------------------|--------------------------|--------------------------|
| dual EnKF | $O(1/\varepsilon^2)$ | $O(1/\log(\varepsilon))$ | 1 |
| Zhang et al. (2021b) | $\tilde{O}(1/\varepsilon^4)$ | $O(1)$ | $O(1/\varepsilon)$ |
| Cassel and Koren (2021) | $\tilde{O}(1/\varepsilon^4)$ | $O(1)$ | $O(1/\varepsilon)$ |
| Krauth et al. (2019) | 1 | $O(1/\varepsilon^2)$ | $O(1/\log(\varepsilon))$ |
| Yang et al. (2019) | 1 | $O(1/\varepsilon^5)$ | $O(\log(1/\varepsilon))$ |

The online approximation of optimal control input is tabulated as Algorithm 2 in Appendix B and an error analysis of the gain appears in Appendix C.3.

Remark 6 *An important observation needs to be made here. The result seems very surprising since τ appears in the denominator, which suggests that choosing a large simulation step size would result in better accuracy. This is happening because of a $\frac{W_\tau}{\tau}$ type term in the error analysis. What is hidden here, is that the error resulting from the discretization of the SDE has not been taken into account in the analysis, and it will yield a $O(\tau)$ type term in the error analysis. Thus the $O(\frac{1}{\tau}) + O(\tau)$ terms will lead to an optimal step size to choose.*

3.3. Comparison of sample complexity to related works

There are two types of errors for which analysis has been reported in recent literature: (i) the error in approximating the optimal value function; and (ii) the error in approximating the optimal gain matrix. Most of these results are for the stationary average cost case in the stochastic setting of the problem or for the infinite-horizon linear quadratic regulator (LQR) in the deterministic ($\sigma = 0$) setting. The quantitative comparisons with prior work are tabulated in Table 2.

In Krauth et al. (2019), an off policy method is used to estimate the Q function for discrete time average cost LQG. A linear function approximation is used with quadratic basis functions. The system is run for some fixed time using an exploration policy. At the end of each episode, the Q function is estimated using least squares. The error bounds in approximating the optimal gain are reported in (Krauth et al., 2019, Theorem 2.2). These results are closest to our work in terms of sample complexity requiring $O(\log(1/\varepsilon))$ training episodes and $O(1/\varepsilon^2)$ simulation time for error of ε (see (Krauth et al., 2019, Theorem 2.2)).

In Yang et al. (2019), a policy gradient algorithm is described. The actor is a gradient descent over the space of gains, where the policy gradient theorem is used to obtain the gradient. Error bounds are obtained for the error in value function (Yang et al., 2019, Theorem 4.3) which is related to error in solution of Riccati equation (Yang et al., 2019, Theorem 4.3). The algorithm needs $O(\log(1/\varepsilon))$ iterations, and a simulation horizon of the order $O(1/\varepsilon)$ for an ε error from the optimal value (Yang et al., 2019, Theorem 4.3).

In [Cassel and Koren \(2021\)](#), a zero order policy gradient algorithm is given for regret minimization in discrete time LQG. The idea is to perturb the gain in random directions to estimate the gradient of the value function with respect to the gain. Based on ([Cassel and Koren, 2021](#), Lemma 6), $\tilde{O}(1/\varepsilon^4)$ samples are needed for gradient estimation and $O(1/\varepsilon)$ gradient descent iterations are needed for ε error in approximating the optimal value.

On the LEQG problem, [Zhang et al. \(2021b\)](#) extends the previous work of [Zhang et al. \(2020\)](#), [Zhang et al. \(2021a\)](#), and studies model free policy gradient methods for finite-horizon discrete-time LEQG. The work utilizes the equivalence between LEQG and linear quadratic min-max game to describe a “double-loop scheme”. The approach is to write the optimization on the space of gains, and then apply a zeroth order policy optimization method to approximate the gradient flow. A sample complexity analysis is given that quantifies the error bounds based on number of iterations and number of samples needed. The algorithm requires $\tilde{O}(1/\varepsilon^4)$ samples to estimate the gradient, and $O(1/\varepsilon)$ of gradient descent iterations for ε error in gain ([Zhang et al., 2021b](#), Theorem 4.3).

The trade-off between EnKF and policy gradient type or least-squares type algorithms is as follows. The latter class of methods typically require multiple iterations (episodes) for simulating a system over a finite time-horizon, albeit with a relatively smaller number of particles, while EnKF needs only a single iteration but with a larger number of particles. Notably, the work in [Yang et al. \(2019\)](#); [Krauth et al. \(2019\)](#); [Lai and Xiong \(2024\)](#); [Yaghmaie et al. \(2023\)](#) needs only a single copy of the system. The EnKF particles are simulated in parallel, giving rise to much more efficient and faster implementation. Moreover, EnKF does not require an initial feasible (stabilizing) gain, while [Krauth et al. \(2019\)](#), [Yang et al. \(2019\)](#), [Yaghmaie et al. \(2023\)](#), [Cassel and Koren \(2021\)](#), [Zhang et al. \(2021b\)](#), [Cui et al. \(2023\)](#), [Lai and Xiong \(2024\)](#) need one.

3.4. Conceptual comparison to path integral control

While the focus of this paper is on designing the interaction term \mathcal{A} in (3a) for the purpose of learning the value function, a related idea is the path integral approach([Kappen \(2005\)](#), [Theodorou and Todorov \(2012\)](#), [Thijssen and Kappen \(2015\)](#), [Williams et al. \(2016\)](#), [Williams et al. \(2018\)](#)) In this class of algorithms, one works with the LQG problem under the assumption that $\Sigma = \lambda D$ for some $\lambda > 0$ (for simplicity we present formulas with $b = \sigma$ and $R = \mathbb{I}$). One simulates multiple trajectories $dX_t^i = (AX_t^i + BU_t^i)dt + dW_t^i$, and approximates the value function as

$$\exp(-V(x, t)) = \mathbb{E} \left[\exp \left(\int_s^T |CX_t|^2 dt - g^U(s, x) \right) \right] \approx \frac{1}{N} \sum_{i=1}^N w_i$$

$$U_s^*(x) - U_s \approx \frac{\sum_{i=1}^N w_i W_\tau^{(i)}}{\tau \sum_{i=1}^N w_i}, \quad w_i := \exp \left(\int_s^T |CX_t^i|^2 dt - g^{U^i}(s, x) \right)$$

with $g^U(s, T) := \int_s^T \frac{1}{2} U_t^T U_t dt + U_t^T dW_t$. The following are key differences between the two approaches: **(i)** In our approach, all particles have equal weight $1/N$. However, importance sampling is well known to suffer from particle degeneracy. The issue becomes severe in higher dimensions and is known as curse of dimensionality, which our algorithm avoids (see [Taghvaei and Mehta \(2023\)](#) for a theoretical comparison). **(ii)** Another major point of distinction with is that the path integral control is a fully model-based algorithm (formula (25) (where implementation of those terms assumes knowledge of B and σ) and Section IV-B in [Williams et al. \(2016\)](#) and Section VI-B in [Williams et al. \(2018\)](#))) while we focus on a simulator-based setting through the design of interactions. Moreover,

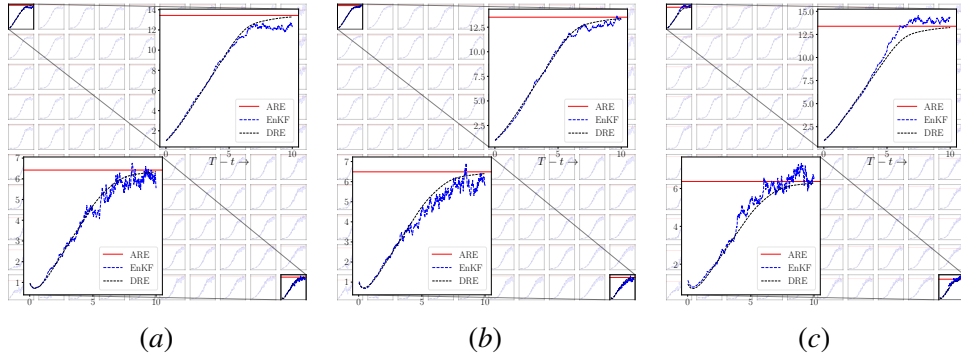


Figure 1: Comparison of the numerical solutions obtained from the EnKF, the DRE, and the ARE. The plots are in order: (a) LQG, (b) LEQG ($\theta > 0$) (c) LEQG ($\theta < 0$).

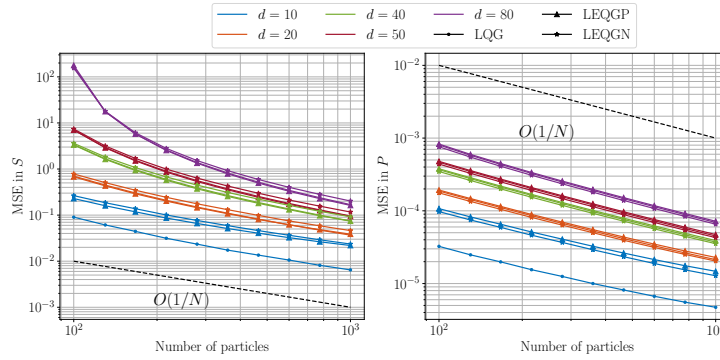


Figure 2: Relative error in approximating the solution of the ARE by the dual EnKF.

MPPI assumes a special relation between control cost and noise which we do not need (see for example, the equation above (24) in Williams et al. (2018) or (Williams et al., 2016, equation (6))). (iii) A third major point is between how trajectories are utilised. Since MPPI needs to iteratively evaluate expectation under the controlled measure, they need to run multiple copies of the system in for each iteration, while we need to run them only once. Our algorithm has interaction between particles, while MPPI uses importance sampling based approaches.

4. Numerical experiments and comparisons

4.1. Numerical illustration of error formulas (9),(10))

An attractive feature of dual EnKF is that with large N , learning rate is inherited from the DRE convergence theory (see formula (10)). A numerical illustration of this formula, showing convergence of the d^2 entries of the P matrix, is depicted in Figure 1. The model is $d = 10$ dimensional where the entries of the A matrix are randomly sampled (see Appendix E.2 for details). Five of the total ten eigenvalues of A have positive real parts for the particular realization used in generating Figure 1.

In order to investigate scaling with increasing state dimension d , a spring mass damper model was introduced in Mohammadi et al. (2019). For this model, all three controllers are evaluated (LQG and LEQG for θ positive and negative). The model and simulation parameters described

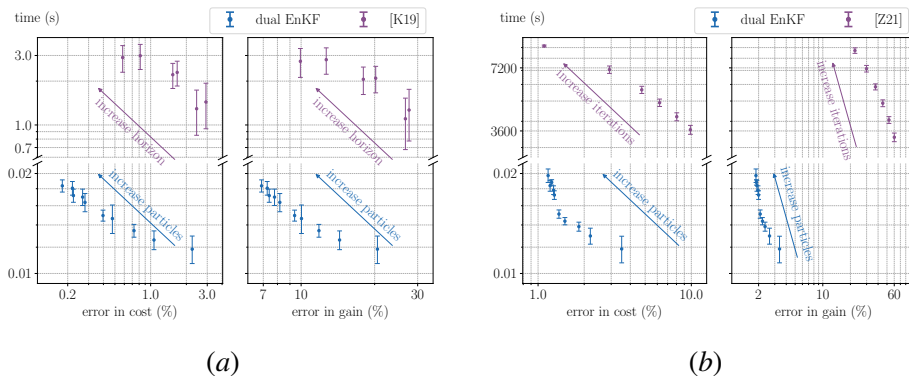


Figure 3: Comparison of dual EnKF with : (a) [K19] for infinite horizon LQG; and (b) [Z21] for finite horizon LEQG. See Section 4.2 for details.

in the Appendix E.1. Figure 2 depicts the scaling as a function of N for the following metrics: $\frac{\mathbb{E}[\|\bar{S}^{(N)} - \bar{S}\|_F^2]}{\|\bar{S}\|_F^2}$ and $\frac{\mathbb{E}[\|\bar{P}^{(N)} - \bar{P}\|_F^2]}{\|\bar{P}\|_F^2}$. Consistent with (9), both the errors go down as $\frac{1}{N}$. Additional results on the performance of the optimal control law appear in the Appendix E.1.

4.2. Numerical comparisons with prior work

Policy optimization: For this study, a three dimensional discrete-time system from Zhang et al. (2021b) is considered. For this model, comparisons are made with the following: (i) Finite-horizon LEQG in Zhang et al. (2021b), denoted [Z21]; and (ii) Average cost LQG in Krauth et al. (2019), denoted [K19]. Comparison is done for relative error in approximation of the optimal gain (with respect to the optimal gain) and relative error in the cost incurred by the control (with respect to the optimal cost) given by the algorithm. Figure 3 depicts the numerically computed relationship between the relative error and the computational time.

Path integral control: We compare relative error in the cost incurred by the control (with respect to the optimal cost) given by the path integral approach (Williams et al., 2018), on the spring mass damper system for various dimensions of the state in Figure 4.

For each algorithm, the error becomes smaller with increasing computational time. For the dual EnKF, this tradeoff is obtained by increasing the number of particles. For [Z21] and [K19], the tradeoff is obtained by increasing the number of iterations and the time horizon. We observe that EnKF needs simulation times which are at least an order of magnitude lower than the other algorithms. See Appendix D for additional information on the optimal control problem and the simulation parameters, and additional discussion on these studies.

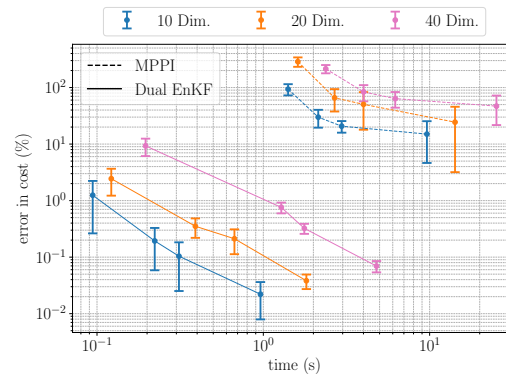


Figure 4: Comparison of dual EnKF with path integral control for spring mass damper system.

References

<https://github.com/wujiduan/Zero-sum-LQ-Games>.

Yasin Abbasi-Yadkori, Nevena Lazic, and Csaba Szepesvari. Model-free linear quadratic control via reduction to expert prediction. In Kamalika Chaudhuri and Masashi Sugiyama, editors, *Proceedings of the Twenty-Second International Conference on Artificial Intelligence and Statistics*, volume 89 of *Proceedings of Machine Learning Research*, pages 3108–3117. PMLR, 16–18 Apr 2019. URL <https://proceedings.mlr.press/v89/abbasi-yadkori19a.html>.

Francis Bach and Vianney Perchet. Highly-smooth zero-th order online optimization. In Vitaly Feldman, Alexander Rakhlin, and Ohad Shamir, editors, *29th Annual Conference on Learning Theory*, volume 49 of *Proceedings of Machine Learning Research*, pages 257–283, Columbia University, New York, New York, USA, 23–26 Jun 2016. PMLR. URL <https://proceedings.mlr.press/v49/bach16.html>.

Matteo Bassei, Xin Guo, Anran Hu, and Yufei Zhang. Logarithmic regret for episodic continuous-time linear-quadratic reinforcement learning over a finite-time horizon. *Journal of Machine Learning Research*, 23(178):1–34, 2022. URL <http://jmlr.org/papers/v23/20-664.html>.

Adrian N. Bishop and Pierre Del Moral. On the stability of kalman–bucy diffusion processes. *SIAM Journal on Control and Optimization*, 55(6):4015–4047, 2017. doi: 10.1137/16M1102707. URL <https://doi.org/10.1137/16M1102707>.

Adrian N Bishop and Pierre Del Moral. On the mathematical theory of ensemble (linear-gaussian) kalman–bucy filtering. *Mathematics of Control, Signals, and Systems*, 35(4):835–903, 2023.

Adrian N. Bishop and Pierre Del Moral. On the stability of matrix-valued Riccati diffusions. *Electronic Journal of Probability*, 24(none):1 – 40, 2019. doi: 10.1214/19-EJP342. URL <https://doi.org/10.1214/19-EJP342>.

R. W Brockett. *Finite dimensional linear systems*. SIAM, 2015.

- Asaf B Cassel and Tomer Koren. Online policy gradient for model free learning of linear quadratic regulators with \sqrt{t} regret. In Marina Meila and Tong Zhang, editors, *Proceedings of the 38th International Conference on Machine Learning*, volume 139 of *Proceedings of Machine Learning Research*, pages 1304–1313. PMLR, 18–24 Jul 2021. URL <https://proceedings.mlr.press/v139/cassel21a.html>.
- Leilei Cui, Tamer Basar, and Zhong-Ping Jiang. A reinforcement learning look at risk-sensitive linear quadratic gaussian control. In Nikolai Matni, Manfred Morari, and George J. Pappas, editors, *Proceedings of The 5th Annual Learning for Dynamics and Control Conference*, volume 211 of *Proceedings of Machine Learning Research*, pages 534–546. PMLR, 15–16 Jun 2023. URL <https://proceedings.mlr.press/v211/cui23c.html>.
- M. H. A. Davis. *Linear estimation and stochastic control*. Chapman and Hall mathematics series. Chapman and Hall, London, 1977. ISBN 0470992158.
- Wendell H. Fleming and H.M. Soner. *Controlled Markov Processes and Viscosity Solutions*. Stochastic Modelling and Applied Probability. Springer New York, NY, 2 edition, 2006. ISBN 978-0-387-31071-8. doi: <https://doi.org/10.1007/0-387-31071-1>.
- Daniel Hernández-Hernández and Pedro Salazar-Sánchez. Risk-sensitive lqg discounted control problems and their asymptotic behavior. *SIAM Journal on Control and Optimization*, 61(3):1136–1161, 2023. doi: [10.1137/21M1459253](https://doi.org/10.1137/21M1459253). URL <https://doi.org/10.1137/21M1459253>.
- A. A. Joshi, A. Taghvaei, P. G. Mehta, and S. P. Meyn. Controlled interacting particle algorithms for simulation-based reinforcement learning. *Systems & Control Letters*, 170:105392, 2022. ISSN 0167-6911. doi: <https://doi.org/10.1016/j.sysconle.2022.105392>. URL <https://www.sciencedirect.com/science/article/pii/S0167691122001694>.
- Hilbert J. Kappen. Linear theory for control of nonlinear stochastic systems. *Phys. Rev. Lett.*, 95:200201, Nov 2005. doi: [10.1103/PhysRevLett.95.200201](https://doi.org/10.1103/PhysRevLett.95.200201). URL <https://link.aps.org/doi/10.1103/PhysRevLett.95.200201>.
- Karl Krauth, Stephen Tu, and Benjamin Recht. Finite-time analysis of approximate policy iteration for the linear quadratic regulator. In H. Wallach, H. Larochelle, A. Beygelzimer, F. d’ Alché-Buc, E. Fox, and R. Garnett, editors, *Advances in Neural Information Processing Systems*, volume 32. Curran Associates, Inc., 2019. URL https://proceedings.neurips.cc/paper_files/paper/2019/file/aaebdb8bb6b0e73f6c3c54a0ab0c6415-Paper.pdf.
- Huibert Kwakernaak and Raphael Sivan. *Linear optimal control systems*. Wiley Interscience, New York, 1972. ISBN 0471511102.
- Jing Lai and Junlin Xiong. Reinforcement learning for linear exponential quadratic gaussian problem. *Systems & Control Letters*, 185:105749, 2024. ISSN 0167-6911. doi: <https://doi.org/10.1016/j.sysconle.2024.105749>. URL <https://www.sciencedirect.com/science/article/pii/S0167691124000379>.
- Daniel Liberzon. *Calculus of Variations and Optimal Control Theory*. Princeton University Press, Princeton, NJ, 2012. ISBN 978-0-691-15187-8. A concise introduction.

- H. Mohammadi, A. Zare, M. Soltanolkotabi, and M. R. Jovanovic. Global exponential convergence of gradient methods over the nonconvex landscape of the linear quadratic regulator. In *2019 IEEE 58th Conference on Decision and Control (CDC)*, pages 7474–7479, December 2019. doi: 10.1109/CDC40024.2019.9029985. ISSN: 2576-2370.
- Hideo Nagai. Risk-sensitive stochastic control. In John Baillieul and Tariq Samad, editors, *Encyclopedia of Systems and Control*, pages 1–9. Springer London, London, 2013. ISBN 978-1-4471-5102-9. doi: 10.1007/978-1-4471-5102-9_233-1. URL https://doi.org/10.1007/978-1-4471-5102-9_233-1.
- Vincent Roulet, Maryam Fazel, Siddhartha Srinivasa, and Zaid Harchaoui. On the convergence of the iterative linear exponential quadratic gaussian algorithm to stationary points. In *2020 American Control Conference (ACC)*, pages 132–137, 2020. doi: 10.23919/ACC45564.2020.9147694.
- Amirhossein Taghvaei and Prashant G. Mehta. A survey of feedback particle filter and related controlled interacting particle systems (cips). *Annual Reviews in Control*, 55:356–378, 2023. ISSN 1367-5788. doi: <https://doi.org/10.1016/j.arcontrol.2023.03.006>. URL <https://www.sciencedirect.com/science/article/pii/S136757882300010X>.
- Evangelos A. Theodorou and Emanuel Todorov. Relative entropy and free energy dualities: Connections to path integral and kl control. In *2012 IEEE 51st IEEE Conference on Decision and Control (CDC)*, pages 1466–1473, 2012. doi: 10.1109/CDC.2012.6426381.
- Sep Thijssen and H. J. Kappen. Path integral control and state-dependent feedback. *Phys. Rev. E*, 91:032104, Mar 2015. doi: 10.1103/PhysRevE.91.032104. URL <https://link.aps.org/doi/10.1103/PhysRevE.91.032104>.
- Grady Williams, Paul Drews, Brian Goldfain, James M. Rehg, and Evangelos A. Theodorou. Aggressive driving with model predictive path integral control. In *2016 IEEE International Conference on Robotics and Automation (ICRA)*, pages 1433–1440, 2016. doi: 10.1109/ICRA.2016.7487277.
- Grady Williams, Paul Drews, Brian Goldfain, James M. Rehg, and Evangelos A. Theodorou. Information-theoretic model predictive control: Theory and applications to autonomous driving. *IEEE Transactions on Robotics*, 34(6):1603–1622, 2018. doi: 10.1109/TRO.2018.2865891.
- Ronald J. Williams. Simple statistical gradient-following algorithms for connectionist reinforcement learning. *Machine Learning*, 8(3):229–256, May 1992. ISSN 1573-0565. doi: 10.1007/BF00992696. URL <https://doi.org/10.1007/BF00992696>.
- Jiduan Wu, Anas Barakat, Ilyas Fatkhullin, and Niao He. Learning zero-sum linear quadratic games with improved sample complexity and last-iterate convergence. URL <https://arxiv.org/abs/2309.04272>. Oct 2023. arXiv:2309.04272.
- Farnaz Adib Yaghmaie, Fredrik Gustafsson, and Lennart Ljung. Linear quadratic control using model-free reinforcement learning. *IEEE Transactions on Automatic Control*, 68(2):737–752, 2023. doi: 10.1109/TAC.2022.3145632.
- Zhuoran Yang, Yongxin Chen, Mingyi Hong, and Zhaoran Wang. Provably global convergence of actor-critic: A case for linear quadratic regulator with ergodic cost. In H. Wallach, H. Larochelle, A. Beygelzimer, F. d’Alché-Buc, E. Fox, and R. Garnett, editors,

Advances in Neural Information Processing Systems, volume 32. Curran Associates, Inc., 2019. URL https://proceedings.neurips.cc/paper_files/paper/2019/file/9713faa264b94e2bf346a1bb52587fd8-Paper.pdf.

Kaiqing Zhang, Bin Hu, and Tamer Basar. Policy Optimization for \mathcal{H}_2 Linear Control with \mathcal{H}_∞ Robustness Guarantee: Implicit Regularization and Global Convergence. In *Proceedings of the 2nd Conference on Learning for Dynamics and Control*, pages 179–190. PMLR, July 2020. URL <https://proceedings.mlr.press/v120/zhang20a.html>. ISSN: 2640-3498.

Kaiqing Zhang, Bin Hu, and Tamer Başar. Policy Optimization for \mathcal{H}_2 Linear Control with \mathcal{H}_∞ Robustness Guarantee: Implicit Regularization and Global Convergence, February 2021a. URL <http://arxiv.org/abs/1910.09496>. arXiv:1910.09496 [cs, eess, math].

Kaiqing Zhang, Xiangyuan Zhang, Bin Hu, and Tamer Basar. Derivative-Free Policy Optimization for Linear Risk-Sensitive and Robust Control Design: Implicit Regularization and Sample Complexity. In *Advances in Neural Information Processing Systems*, volume 34, pages 2949–2964. Curran Associates, Inc., 2021b. URL <https://proceedings.neurips.cc/paper/2021/hash/1714726c817af50457d810aae9d27a2e-Abstract.html>.

Appendix A. Theory

A.1. Simulator

We assume access to a simulator but not explicit knowledge of the system matrices A, B . The simulator-based setting is widely applicable in RL, for instance, in the ATARI games, open AI gym, MuJoCo and other such environments. In these settings, the transition probabilities are not explicitly known but one is allowed to sample the trajectory by running a simulation. In many scenarios, e.g., tic-tac-toe or chess or the game of go, transition probabilities are exactly known (these are used to construct the game). However, it is a common RL practice to approximately solve the dynamic programming equation only using simulations (having the computer play the game). We are doing something similar for LQ optimal control problem.

For the linear quadratic problems, previously published works by various research groups have also focused on the simulation-based setting (Remark 2). The distinction and the advantage of our approach is that careful design of interactions between simulations is shown to drastically improve computational time. The original idea of our work is that, at least for LQ problems, substantial gains can be made by coupling the simulations. For example, standard ARE solvers (in scipy) fail for large dimensions ($d = 200$) but an EnKF can still give a solution. EnKF is the preferred algorithm in data assimilation applications where the state-space is truly large.

Our approach is very relevant in the dynamical systems community where there many instances where one has a high fidelity simulator of the system, but obtaining and analytically solving an exact model is very hard, for instance, weather systems, fluid or aerodynamic simulations, and our approach is the first step to providing controllers for such systems using interacting particle systems, without the explicit use of models.

There is however, a concern about robustness. If the real plant differs from simulations then one would need some online strategy to estimate and correct for such errors.

A.2. Log transform

The value function $\{v_t(x) : 0 \leq t \leq T, x \in \mathbb{R}^d\}$ is defined as follows

$$v_t(x) := \min_{U(\cdot) \in \mathcal{U}} \{J_T(U) - J_t(U)\}$$

s.t. (1) and $X_0 = x$.

Taking inspiration from literature for using log transform risk sensitive control (Fleming and Soner, 2006, Chapter 6), we define a map $\psi : \mathbb{R} \rightarrow \mathbb{R}$ so that

$$p_t(x) := \frac{\psi(v_t(x))}{\int \psi(v_t(x)) dx}, \quad 0 \leq t \leq T, x \in \mathbb{R}^d \tag{13}$$

is a valid probability density function. The bijection ψ is selected as

$$\psi(z) := \begin{cases} \exp(-z); & \text{LQG} \\ \exp(-|\theta|z); & \text{LEQG} \end{cases} \tag{14}$$

Due to the quadratic nature of the value function, p_t is the Gaussian density $\mathcal{N}(0, S_t)$. The idea is to approximate p_t using an ensemble of simulations, then obtain P_t to find the optimal control.

Table 3: Vector fields for (15).

| | $\mathcal{I}_t(z; n_t, S_t)$ | $\mathcal{C}_t(z; n_t, S_t)$ | $\text{Cov}(\eta)$ |
|----------------------|--|---------------------------------------|---------------------------|
| LQG | $\frac{1}{2}S_t C^T C(z + n_t)$ | $\frac{1}{2}\Sigma S_t^{-1}(z - n_t)$ | R^{-1} |
| LEQG $\theta > 0$ | $\frac{ \theta }{2}S_t C^T C(z + n_t)$ | $\Sigma S_t^{-1}(z - n_t)$ | $(\sqrt{ \theta }R)^{-1}$ |
| LEQG $\theta < 0$ | | 0 | |

A.3. Mean field system

Define a stochastic process $Y = \{Y_t \in \mathbb{R}^d : 0 \leq t \leq T\}$ as a solution of the following backward (in time) SDE:

$$dY_t = AY_t dt + Bd\bar{\eta}_t + \sigma d\bar{W}_t + (\mathcal{I}_t(Y_t; \bar{n}_t, \bar{S}_t) + \mathcal{C}_t(Y_t; \bar{n}_t, \bar{S}_t))dt \quad (15a)$$

$$Y_T \sim \mathcal{N}(0, S_T) \quad (15b)$$

where $\eta = \{\eta_t \in \mathbb{R}^m : 0 \leq t \leq T\}$ is a B.M. with a suitably chosen covariance matrix, $\mathcal{I}_t(\cdot; \cdot), \mathcal{C}_t(\cdot; \cdot)$ is a suitably chosen vector field, and \bar{p}_t is the density of Y .

Proposition 7 Consider the mean-field process (15). Suppose $\text{Cov}(\eta)$, \mathcal{I} and \mathcal{C} is selected according to Table 3. Then, $\bar{p}_t = p_t$, $\forall t \in [0, T]$, where \bar{p}_t is the probability density function of Y_t and p_t is defined in (13) in terms of the value function. The optimal control is expressed as a function of \bar{p}_t according to

$$U_t^* = \begin{cases} R^{-1}B^T \nabla \log \bar{p}_t(X_t); & \text{LQG} \\ (|\theta|R)^{-1}B^T \nabla \log \bar{p}_t(X_t); & \text{LEQG} \end{cases}$$

Proof See Section A.5. ■

Note that the \mathcal{A}_t in (7) is the sum of \mathcal{I} and \mathcal{C} . These quantities are expressed individually, since \mathcal{I} depends entirely on parameters obtained from the LQ cost, and \mathcal{C} depends entirely on parameters appearing in the coefficient for noise σ .

A.4. Finite-N approximation

The mean-field process (15) is empirically approximated by simulating a system of controlled interacting particles $\{Y_t^i \in \mathbb{R}^d : 0 \leq t \leq T, i = 1, \dots, N\}$ according to (3).

A.5. Details of mean field system

What we need to show is that $Y_t \sim \mathcal{N}(0, S_t)$ for each $0 \leq t \leq T$. Upon substitution of \mathcal{I} and \mathcal{C} , the mean field system (15) for Y becomes, for LQG

$$dY_t = AY_t dt + Bd\bar{\eta}_t + \frac{1}{2}\bar{S}_t C^T (CY_t + C\bar{n}_t)dt + \frac{1}{2}\sigma\sigma^T \bar{S}_t^{-1}(Y_t - \bar{n}_t)dt + \sigma d\bar{W}_t,$$

and for LEQG for $\theta > 0$

$$dY_t = AY_t dt + Bd\bar{\eta}_t + \sigma d\bar{W}_t + \frac{\theta}{2} \bar{S}_t C^T (CY_t + C\bar{n}_t) dt + \sigma \sigma^T \bar{S}_t^{-1} (Y_t - \bar{n}_t) dt,$$

for $\theta < 0$

$$dY_t = AY_t dt + Bd\bar{\eta}_t + \sigma d\bar{W}_t - \frac{\theta}{2} \bar{S}_t C^T (CY_t + C\bar{n}_t) dt,$$

where

$$\bar{n}_t = \mathbb{E}[Y_t], \bar{S}_t = \mathbb{E}[(Y_t - \bar{n}_t)(Y_t - \bar{n}_t)^T], Y_0 \sim \mathcal{N}(0, P_T^{-1}), dW_t \sim \mathcal{N}(0, \mathbb{I} dt)$$

and η is a Brownian motion with covariance as in Table 3. Then we have for LQG

$$\begin{aligned} \dot{\bar{n}}_t &= (A + \bar{S}_t C^T C) \bar{n}_t, \\ \dot{\bar{S}}_t &= A\bar{S}_t + \bar{S}_t A^T + \bar{S}_t C^T C \bar{S}_t - BR^{-1}B^T, \end{aligned}$$

and for LEQG

$$\begin{aligned} \dot{\bar{n}}_t &= (A + \frac{|\theta|}{2} \bar{S}_t C^T C) \bar{n}_t \\ \dot{\bar{S}}_t &= A\bar{S}_t + \bar{S}_t A^T + |\theta| \bar{S}_t C^T C \bar{S}_t - \frac{1}{|\theta|} (BR^{-1}B^T - \theta \sigma \sigma^T). \end{aligned}$$

The terminal conditions are for all cases, $\bar{n}_T = 0$ and $\bar{S}_T = S_T$. Since \bar{n}_T is zero, then $\bar{n}_t = 0$ for all $0 \leq t \leq T$. And since \bar{S}_t follows the same ODE as S_t (in (5)) and has the same terminal condition, it must be that $\bar{S}_t = S_t$ for all $0 \leq t \leq T$.

Finally, Y is a Gaussian process since the SDE (15) is an Ornstein-Uhlenbeck process with a Gaussian terminal condition.

Appendix B. Algorithms for implementation

Algorithm 1 is the offline algorithm to estimate the \mathcal{Q} function, and Algorithm 2 is the online algorithm to compute the optimal control.

Appendix C. Error Analysis

C.1. Obtaining bounds in (9)

We get the bound (9) from (Bishop and Moral, 2019, equation (2.10)) (where the reader may also refer to Section 1.1, equation (1.4) and equation (3.7) of Bishop and Moral (2019) for more clarity). In the following, we go through the steps of obtaining the bounds (9) using the aforementioned results from Bishop and Moral (2019). The assumption $N \geq d + 1$ is justified in the end of (Bishop and Moral, 2019, Section 3.1).

We analyze the SDE (15), which is the the mean field system for the particle system (3). We will analyze the system forward in time. To that end, consider the following mean field system for LQG

$$dH_t = -AH_t dt + Bd\eta_t - \frac{1}{2} \Omega_t C^T (CH_t + Ch_t) dt - \frac{1}{2} \sigma \sigma^T \Omega_t^{-1} (H_t - h_t) dt + \sigma dW_t,$$

Algorithm 1 [offline] dual EnKF algorithm to approximate empirical Q function

Input: Simulation time T , simulation step-size τ , number of particles N , simulator \mathcal{S} for (1) (see Definition 1), terminal covariance S_T from (5), running cost function C , and control cost matrix R , and risk parameter θ if applicable, the function \mathcal{A} and covariance $\text{Cov}(\eta)$ from (7) and (6).

- 1: **return** $\{P_k^{(N)}, \mathcal{Q}^{(N)}(\cdot, \cdot; k, \tau) : k = 0, 1, 2, \dots, \frac{T}{\tau} - 1\}$
 - 2: $T_F = \frac{T}{\tau}$
 - 3: Initialize $\{Y_{T_F}^i\}_{i=1}^N \stackrel{\text{i.i.d.}}{\sim} \mathcal{N}(0, S_T)$
 - 4: calculate $n_{T_F}^{(N)} = N^{-1} \sum_{i=1}^N Y_{T_F}^i$
 - 5: calculate $S_{T_F}^{(N)} = (N-1)^{-1} \sum_{i=1}^N (Y_{T_F}^i - n_{T_F}^{(N)})(Y_{T_F}^i - n_{T_F}^{(N)})^\top$
 - 6: **for** $k = T_F$ to 1 **do**
 - 7: Calculate $A_k^{(N)} = \mathcal{A}(Y_k^i, n_t^{(N)}, S_t^{(N)})$
 - 8: **for** $i = 1$ to N **do**
 - 9: $\Delta \eta_k^i \stackrel{\text{i.i.d.}}{\sim} \mathcal{N}(0, \text{Cov}(\eta)\tau)$
 - 10: $\Delta Y_k^i = \mathcal{S}(Y_k^i, \Delta \eta_k^i, \tau) + A_k^{(N)}\tau$
 - 11: $Y_{k-1}^i = Y_k^i - \Delta Y_k^i$
 - 12: **end for**
 - 13: Calculate $n_{k-1}^{(N)} = N^{-1} \sum_{i=1}^N Y_{k-1}^i$
 - 14: Calculate $S_{k-1}^{(N)} = (N-1)^{-1} \sum_{i=1}^N (Y_{k-1}^i - n_{k-1}^{(N)})(Y_{k-1}^i - n_{k-1}^{(N)})^\top$
 - 15: Obtain $P_{k-1}^{(N)}$ from $S_{k-1}^{(N)}$ using (5), and $\mathcal{Q}^{(N)}(x, a; k, \tau)$ using (11).
 - 16: **end for**
-

and for LEQG with $\theta > 0$

$$dH_t = -AH_t dt + Bd\eta_t + \sigma dW_t - \frac{\theta}{2} \Omega_t C^\top (CH_t + Ch_t) dt - \sigma \sigma^\top \Omega_t^{-1} (H_t - h_t) dt,$$

for LEQG with $\theta < 0$

$$dH_t = -AH_t dt + Bd\eta_t + \sigma dW_t + \frac{\theta}{2} \Omega_t C^\top (CH_t + Ch_t) dt,$$

where

$$h_t = \mathbb{E}[H_t], \quad \Omega_t = \mathbb{E}[(H_t - h_t)(H_t - h_t)^\top], \quad H_0 \sim \mathcal{N}(0, P_T^{-1}), \quad dW_t \sim \mathcal{N}(0, \text{Id}t)$$

and η is a Brownian motion with covariance as in Table 3. Then we have for LQG

$$\begin{aligned} \dot{h}_t &= -(A + \Omega_t C^\top C) h_t \\ \dot{\Omega}_t &= -A\Omega_t - \Omega_t A^\top - \Omega_t C^\top C \Omega_t + BR^{-1}B^\top \end{aligned}$$

and for LEQG

$$\begin{aligned} \dot{h}_t &= -(A + \frac{|\theta|}{2} \Omega_t C^\top C) h_t \\ \dot{\Omega}_t &= -A\Omega_t - \Omega_t A^\top - |\theta| \Omega_t C^\top C \Omega_t + \frac{1}{|\theta|} (BR^{-1}B^\top - \theta \sigma \sigma^\top) \end{aligned}$$

Algorithm 2 [online] dual EnKF algorithm to calculate optimal control

Input: Simulation time T , simulation step-size τ , number of averaging evaluations N_e , empirical Q-function $\mathcal{Q}^{(N)}(x, a, \tau)$ (see Definition 5), $\{e_i\}_{i=1}^m$ the standard basis of \mathbb{R}^m .

- 1: **return** optimal control input $\{\hat{U}_k^{(N)} \in \mathbb{R}^m : k = 0, 1, 2, \dots, \frac{T}{\tau} - 1\}$.
- 2: Define $T_F := \frac{T}{\tau}$
- 3: **for** $k = 0$ to $T_F - 1$ **do**
- 4: Observe state of the system, denoted x_k
- 5: Define $y_k := P_k^{(N)} x_k, M_1 := 0$
- 6: **for** $j = 1$ to N_e **do**
- 7: $M_1 \leftarrow M_1 + \mathcal{Q}^{(N)}(x_k, 0, \tau)$
- 8: **end for**
- 9: $M_1 \leftarrow (N_e)^{-1} M_1$
- 10: **for** $i = 1$ to m **do**
- 11: Define $M_2 := 0$
- 12: **for** $j = 1$ to N_e **do**
- 13: $M_2 \leftarrow M_2 + \mathcal{Q}^{(N)}(x_k, R^{-1} e_i, \tau)$
- 14: **end for**
- 15: $M_2 \leftarrow (N_e)^{-1} M_2$
- 16: $\langle \hat{U}_k^{(N)}, e_i \rangle = M_2 - M_1 - \frac{1}{2} (R^{-1})_{ii} \tau$
- 17: **end for**
- 18: Apply control $\hat{U}_k^{(N)}$ to the true system
- 19: **end for**

If the system is implemented using N particles as follows for LQG,

$$\begin{aligned} dH_t^i &= -AH_t^i dt + Bd\eta_t^i - \frac{1}{2} \Omega_t^{(N)} C^T C (H_t^i + h_t^{(N)}) dt \\ &\quad - \frac{1}{2} \sigma \sigma^T (\Omega_t^{(N)})^{-1} (H_t^i - h_t^{(N)}) dt + \sigma dW_t^i \end{aligned}$$

and for LEQG for $\theta > 0$

$$\begin{aligned} dH_t^i &= -AH_t^i dt + Bd\eta_t^i + \sigma dW_t^i - \frac{\theta}{2} \Omega_t^{(N)} C^T (CH_t^i \\ &\quad + Ch_t^{(N)}) dt - \sigma \sigma^T (\Omega_t^{(N)})^{-1} (H_t^i - h_t^{(N)}) dt \end{aligned}$$

for $\theta < 0$

$$dH_t^i = -AH_t^i dt + Bd\eta_t^i + \sigma dW_t^i + \frac{\theta}{2} \Omega_t^{(N)} C^T (CH_t^i + Ch_t^{(N)}) dt$$

where

$$h_t^{(N)} = \frac{1}{N} \sum_{i=1}^N H_t^i, \quad \Omega_t^{(N)} = \frac{1}{N-1} \sum_{i=1}^N (H_t^i - h_t^{(N)}) (H_t^i - h_t^{(N)})^T$$

and η_t^i are iid copies of η . Then we have The time-evolution for $\Omega_t^{(N)}$ is obtained by the application of the Itô rule to its definition (Bishop and Del Moral, 2023, Proposition 4.2)

$$d\Omega_t^{(N)} = (-A\Omega_t^{(N)} - \Omega_t^{(N)}A^\top - \Omega_t^{(N)}C^\top C\Omega_t^{(N)} + B_1R_1^{-1}B_1^\top)dt + \frac{1}{\sqrt{N}}dM_t \quad (16a)$$

$$dM_t = \frac{1}{\sqrt{N}} \sum_{i=1}^N (e_t^i(Bd\eta_t^i + \sigma dW_t^i)^\top + (Bd\eta_t^i + \sigma dW_t^i)(e_t^i)^\top), \quad e_t^i := H_t^i - h_t^{(N)} \quad (16b)$$

Remark 8 Observe that $\Omega_t = S_{T-t}$ and $\Omega_t^{(N)} = S_{T-t}^{(N)}$.

Finally, we get the bound (9) from (Bishop and Moral, 2019, equation (2.10)). To see how to apply the result to our case, notice that $\Omega_t^{(N)}$ follows the same dynamics as (Bishop and Moral, 2019, equation (3.7)) (where the reader may refer Section 1.1 (with particular emphasis on equation (1.4)) of Bishop and Moral (2019) for better clarity).

C.2. Obtaining bounds in (10)

These proofs are largely based on the proofs in Joshi et al. (2022).

Notation: Let $S_+^d \subset S^d \subset \mathbb{R}^{d \times d}$ denote the set of symmetric positive definite matrices and symmetric matrices respectively. Let $\langle Q_1, Q_2 \rangle := \text{Tr}(Q_1 Q_2^\top)$ denote the Frobenius inner product for $Q_1, Q_2 \in \mathbb{R}^{d \times d}$. Then $\|\cdot\|_F := \sqrt{\langle Q_1, Q_1 \rangle}$.

In this section (that is, in Appendix C.2), for LEQG, we redefine $C \leftarrow \sqrt{|\theta|}C$ to keep notation the same for all problems for further analysis.

From Appendix C.1 we know that Ω_t satisfies the Riccati equation

$$\dot{\Omega}_t = \text{Ricc}(\Omega_t) := -A\Omega_t - \Omega_t A^\top - \Omega_t C^\top C \Omega_t + \Sigma_B, \quad (17)$$

where $\Sigma_B := BR^{-1}B^\top$ for LQG and $\Sigma_B := |\theta|^{-1}(BR^{-1}B^\top - \theta\Sigma)$ for LEQG with $\Sigma := \sigma\sigma^\top$. From (16) we know that

$$d\Omega_t^{(N)} = \text{Ricc}(\Omega_t^{(N)})dt + \frac{1}{\sqrt{N}}dM_t, \quad (18)$$

where $\{M_t : t \geq 0\}$ is a martingale given by

$$dM_t = \frac{1}{N-1} \sum_{i=1}^N (e_t^i(Bd\eta_t^i + \sigma dW_t^i)^\top + (Bd\eta_t^i + \sigma dW_t^i)(e_t^i)^\top), \quad e_t^i := H_t^i - h_t^{(N)}$$

with quadratic variation

$$d\langle M \rangle_t = (\text{Tr}(\Sigma_B) + \Sigma)\Omega_t^{(N)} + (\Sigma_B + \Sigma)\text{Tr}(\Omega_t^{(N)}) + (\Sigma_B + \Sigma)\Omega_t^{(N)} + \Omega_t^{(N)}(\Sigma_B + \Sigma)$$

Let $\phi(t, Q)$ denote the semigroup associated with the Riccati equation such that for any positive definite matrix $Q \in S_+^d$,

$$\frac{\partial \phi}{\partial t}(t, Q) = \text{Ricc}(\phi(t, Q)), \quad \phi(0, Q) = Q.$$

We define the first-order and the second-order derivatives which are the linear and bilinear operators $\frac{\partial\phi}{\partial Q}(t, Q) : S^d \rightarrow S^d$ and $\frac{\partial^2\phi}{\partial Q^2}(t, Q) : S^d \times S^d \rightarrow S^d$ respectively as

$$\begin{aligned}\frac{\partial\phi}{\partial Q}(t, Q)(Q_1) &:= \left. \frac{d}{d\epsilon} \right|_{\epsilon=0} \phi(t, Q + \epsilon Q_1) \\ \frac{\partial^2\phi}{\partial Q^2}(t, Q)(Q_1, Q_1) &:= \left. \frac{d^2}{d\epsilon^2} \right|_{\epsilon=0} \phi(t, Q + \epsilon Q_1).\end{aligned}$$

We denote by $\|\frac{\partial\phi}{\partial Q}(t, Q)\|_{F,F}$ and $\|\frac{\partial^2\phi}{\partial Q^2}(t, Q)\|_{F,F}$ induced-norm of these operators with respect to the Frobenius norm. The following lemma is an intermediate result.

Lemma 9 For Ω_t and $\Omega_t^{(N)}$ defined in (17) and (18) respectively, the following is true,

$$\begin{aligned}\Omega_t^{(N)} - \Omega_t &= \frac{1}{\sqrt{N}} \int_0^t \frac{\partial\phi}{\partial Q}(t-s, \Omega_s^{(N)})(dM_s) \\ &\quad + \frac{1}{2N} \int_0^t \frac{\partial^2\phi}{\partial Q^2}(t-s, \Omega_s^{(N)})(dM_s, dM_s) + \phi(t, \Omega_0^{(N)}) - \phi(t, \Omega_0)\end{aligned}\tag{19}$$

Proof We see that

$$\begin{aligned}\Omega_t^{(N)} - \Omega_t &= \phi(0, \Omega_t^{(N)}) - \phi(t, \Omega_0) \\ &= \phi(0, \Omega_t^{(N)}) - \phi(t, \Omega_0^{(N)}) + \phi(t, \Omega_0^{(N)}) - \phi(0, \Omega_0) \\ &= \int_0^t d_s\phi(t-s, \Omega_s^{(N)}) + \phi(t, \Omega_0^{(N)}) - \phi(t, \Omega_0).\end{aligned}$$

Evaluating the differential we have,

$$\begin{aligned}d_s\phi(t-s, \Omega_s^{(N)}) &= -\frac{\partial\phi}{\partial t}(t-s, \Omega_s^{(N)})ds + \frac{\partial\phi}{\partial Q}(t-s, \Omega_s^{(N)})(d\Omega_s^{(N)}) \\ &\quad + \frac{1}{2} \frac{\partial^2\phi}{\partial Q^2}(t-s, \Omega_s^{(N)})(d\Omega_s^{(N)}, d\Omega_s^{(N)}),\end{aligned}$$

where we used the identity $\frac{\partial\phi}{\partial t}(t, Q) = \frac{\partial\phi}{\partial Q}(t, Q)(\text{Ricc}(Q))$. ■

We need the following assumption to use the aforementioned lemma to arrive at the desired result.

Assumption 2 Consider the semigroup corresponding to the Riccati equation (17). There are positive constants c_1 , c_2 , and λ such that $\forall Q \in S_+^d$:

$$\left\| \frac{\partial\phi}{\partial Q}(t, Q) \right\|_{F,F} \leq c_1 e^{-2\lambda t}, \quad \left\| \frac{\partial^2\phi}{\partial Q^2}(t, Q) \right\|_{F,F} \leq c_2 e^{-2\lambda t}.$$

Exponential decay holds for (A, B) controllable and (A, C) observable, (Bishop and Del Moral, 2023, Section 2). However, the for the constants c_1 and c_2 to be the same for initial Q , see (Bishop and Del Moral, 2017, Section 4.2) for detailed analysis of the Riccati equation under the additional assumption that the matrix C is full-rank.

Proposition 10 *If Assumption 2 holds, the the following upper-bound (repeated from (10)) is true*

$$\mathbb{E}[\|S_t^{(N)} - S_t\|_F] \leq \frac{C_5}{\sqrt{N}} + C_6 e^{-2\lambda(T-t)} \mathbb{E}[\|S_T^{(N)} - S_T\|_F],$$

where C_5, C_6 are time-independent positive constants.

Proof Using triangle inequality for norm on (19) we get

$$\mathbb{E}[\|\Omega_t^{(N)} - \Omega_t\|_F] \leq \frac{r_1}{\sqrt{N}} + \frac{r_2}{2N} + r_3$$

where we define

$$\begin{aligned} r_1 &:= \mathbb{E} \left[\left\| \int_0^t \frac{\partial \phi}{\partial Q}(t-s, \Omega_s) (dM_s) \right\|_F \right] \\ r_2 &:= \mathbb{E} \left[\int_0^t \left\| \frac{\partial^2 \phi}{\partial Q^2}(t-s, \Omega_s) (dM_s, dM_s) \right\|_F \right] \\ r_3 &:= \mathbb{E} \left[\left\| \phi(t, \Omega_0^{(N)}) - \phi(t, \Omega_0) \right\|_F \right] \end{aligned}$$

Now we get bounds for r_1, r_2 and r_3 . For r_1 ,

$$\begin{aligned} r_1 &\leq \left[\mathbb{E} \left[\left\| \int_0^t \frac{\partial \phi}{\partial Q}(t-s, \Omega_s) (dM_s) \right\|_F^2 \right] \right]^{\frac{1}{2}} \\ &= \left[\int_0^t \mathbb{E} \left[\left\| \frac{\partial \phi}{\partial Q}(t-s, \Omega_s) (dM_s) \right\|_F^2 \right] \right]^{\frac{1}{2}} \\ &\leq \left[\int_0^t \mathbb{E} \left[\left\| \frac{\partial \phi}{\partial Q}(t-s, \Omega_s) \right\|_{F,F}^2 \|dM_s\|_F^2 \right] \right]^{\frac{1}{2}} \\ &\leq \left[\int_0^t 4c_1^2 e^{-4\lambda(t-s)} \text{Tr}(\Sigma_B + \Sigma) \mathbb{E}[\text{Tr}(\Omega_s^{(N)})] ds \right]^{\frac{1}{2}} \end{aligned}$$

where in the first inequality we used Jensen's inequality, for the second inequality we used Itô isometry in the second step, and Assumption 2 in the last inequality. For r_2 we used Assumption 2 to see that

$$\begin{aligned} r_2 &\leq \mathbb{E} \left[\int_0^t \left\| \frac{\partial^2 \phi}{\partial Q^2}(t-s, \Omega_s) \right\|_F \|dM_s\|_F^2 \right] \\ &\leq \int_0^t 4c_2 e^{-2\lambda(t-s)} \text{Tr}(\Sigma_B + \Sigma) \mathbb{E}[\text{Tr}(\Omega_s^{(N)})] ds \end{aligned}$$

For the bounds on r_3 we use the bounds on the first derivative in Assumption 2 to get

$$r_3 \leq c_1 e^{-2\lambda t} \mathbb{E}[\|\Omega_0^{(N)} - \Omega_0\|_F]$$

Upon using the bound $\mathbb{E}[\text{Tr}(\Omega_t^{(N)})] \leq \text{Tr}(\Omega_t)$ from (Bishop and Del Moral, 2023, Theorem 5.2), and from exponential convergence of Ω_t to $\bar{\Omega}$, there exists $E_0 \in (0, \infty)$ such that $\text{Tr}(\Omega_t) \leq \sup_{t \geq 0} \text{Tr}(\Omega_t) \leq E_0$ we get that

$$\mathbb{E}[\|\Omega_t^{(N)} - \Omega_t\|_F] \leq (c_1 + c_2\sqrt{\epsilon})\sqrt{\epsilon} + c_1 e^{-2\lambda t} \mathbb{E}[\|\Omega_0^{(N)} - \Omega_0\|_F]$$

where $\epsilon := \frac{E_0 \text{Tr}(\Sigma_B + \Sigma)}{\lambda N}$. Making a change of variable from t to $T - t$ and recalling Remark 8 concludes the proof. \blacksquare

C.3. Obtaining bounds in (12)

Fix a time $t \in [0, T]$ and $x \in \mathbb{R}^d$. Fix a step size τ . Recall the Q function is, with $y := P_t^{(N)} x$,

$$\begin{aligned} \mathcal{Q}(x, a, \tau) &= y^T \mathcal{S}(x, a, \tau) + \left(\frac{1}{2}|Cx|^2 + \frac{1}{2}a^T Ra\right)\tau \\ &= y^T ((Ax + Ba)\tau + \sigma \Delta W) + \left(\frac{1}{2}|Cx|^2 + \frac{1}{2}a^T Ra\right)\tau \end{aligned}$$

with $\Delta W \sim \mathcal{N}(0, \mathbb{I}\tau)$. To obtain the optimal control, we minimize the Hamiltonian with respect to a after substituting the value of the momentum y in terms of x . Define $K_t := -R^{-1}B^T P_t$, $U_t^{\text{opt}} := K_t x$, $K_t^{(N)} := -R^{-1}B^T P_t^{(N)}$ and $U_t^{(N)} := K_t^{(N)} x$. The first step is getting an expression for $\hat{U}_t^{(N)}$. The Q function is,

$$\begin{aligned} \mathcal{Q}(x, a, \tau) &= \frac{1}{2}a^T Ra\tau + (x^T P_t^{(N)} B\tau)a + \alpha^T \Delta W + \varphi(x) \\ \varphi(x) &:= \frac{1}{2}x^T (Q\tau + P_t^{(N)} A\tau + A^T P_t^{(N)} \tau)x, \quad \alpha := \sigma^T P_t^{(N)} x \end{aligned}$$

To be consistent with notation used in the algorithm, define

$$\begin{aligned} M_1 &:= \frac{1}{N_e} \sum_{i=1}^{N_e} \mathcal{Q}(x, 0, \tau) = \varphi(x) + \alpha^T (\Delta W)_1 \\ (\Delta W)_1 &:= \frac{1}{N_e} \sum_{i=1}^{N_e} (\Delta W) \sim \mathcal{N}(0, \frac{\tau}{N_e}) \\ M_2^i &:= \frac{1}{N_e} \sum_{i=1}^{N_e} \mathcal{Q}(x, R^{-1}e_i, \tau) \end{aligned}$$

where the summation denotes that each call of the Hamiltonian function produces an independent realization of the random variable ΔW . Now,

$$\mathcal{Q}(x, R^{-1}e_i, \tau) = \frac{1}{2}(R^{-1})_{ii}\tau + \beta_i\tau + \alpha^T \Delta W + \varphi(x)$$

where $\beta_i := e_i^T (R^{-1}B^T P_t^{(N)} x) = \langle U_t^{(N)}, e_i \rangle$, which gives

$$\begin{aligned} \mathcal{Q}(x, R^{-1}e_i, \tau) - \frac{1}{2}(R^{-1})_{ii}\tau - M_1 &= \beta_i\tau + \alpha^T \Delta W + (\varphi(x) - M_1) \\ &= \beta_i\tau + \alpha^T (\Delta W - (\Delta W)_1) \end{aligned}$$

Therefore,

$$M_2^i - \frac{1}{2}(R^{-1})_{ii}\tau - M_1 = \beta_i\tau + \alpha^\top((\Delta W)_2 - (\Delta W)_1).$$

where again $(\Delta W)_2 := \frac{1}{N_e} \sum_{i=1}^{N_e} (\Delta W) \sim \mathcal{N}(0, \frac{\tau}{N_e})$ and the summation similarly denotes that each function call of the Hamiltonian gives an independent realization of ΔW . Since by definition, $\langle \hat{U}_t^{(N)}, e_i \rangle = (M_2^i - \frac{1}{2}(R^{-1})_{ii}\tau - M_1) \frac{1}{\tau}$ we have

$$\langle \hat{U}_t^{(N)}, e_i \rangle = \langle U_t^{(N)}, e_i \rangle + \alpha^\top \left(\frac{(\Delta W)_2 - (\Delta W)_1}{\tau} \right). \quad (20)$$

Define

$$\omega := P_t^{(N)} \sigma \xi, \quad \xi := \left(\frac{(\Delta W)_2 - (\Delta W)_1}{\tau} \right) \sim \mathcal{N}(0, \frac{2}{N_e \tau}).$$

Then from (20) we see that $\hat{U}_t^{(N)} = U_t^{(N)} + (\mathbf{1}\omega^\top)x$. Thus, we define $\hat{K}_t^{(N)} := K_t^{(N)} + \mathbf{1}\omega^\top$, where $\mathbf{1}$ denotes the vector with each entry equal to 1, to get $\hat{U}_t^{(N)} = \hat{K}_t^{(N)}x$. Now we give the mean square error between $\hat{K}_t^{(N)}$ and K_t as

$$\frac{1}{2} \mathbb{E} \left[\|\hat{K}_t^{(N)} - K_t\|^2 \right] \leq \mathbb{E} \left[\|\hat{K}_t^{(N)} - K_t^{(N)}\|^2 \right] + \mathbb{E} \left[\|K_t^{(N)} - K_t^*\|^2 \right]$$

The first term can be estimated as

$$\begin{aligned} \mathbb{E} \left[\|K_t^{(N)} - K_t\|^2 \right] &= \mathbb{E} \left[\|\mathbf{1}^\top \omega\|^2 \right] = n \mathbb{E} \left[\|P_t^{(N)} \sigma \xi\|^2 \right] \\ &\leq 2n \mathbb{E} \left[\|P_t^{(N)} - P_t\|^2 \|\sigma\|^2 |\xi|^2 \right] + 2n \|P_t\|^2 \|\sigma\|^2 \mathbb{E} [|\xi|^2] \\ &= \frac{2n}{N_e \tau} (\tilde{C}_1 + \tilde{C}_2) \end{aligned}$$

where we used (9) and the fact that ξ and $P_t^{(N)}$ are independent random variables, and exponential convergence of P_t to P_∞ ensures a uniform bound on $\|P_t\|$. The second term can be estimated as

$$\begin{aligned} \mathbb{E} \left[\|K_t^{(N)} - K_t\|^2 \right] &= \mathbb{E} \left[\|R^{-1} B^\top (P_t^{(N)} - P_t)\|^2 \right] \\ &\leq \|R^{-1} B^\top\|^2 \frac{\tilde{C}_3}{N} \end{aligned}$$

using properties of matrix norms and equivalence of $\|\cdot\|$ and $\|\cdot\|_F$.

Appendix D. Simulation details for numerical comparisons

D.1. Policy optimization

We compare our algorithm with [K19] and [Z21]. Codes for [K19] were found in the supplementary material of their paper [Krauth et al. \(2019\)](#), while codes for [Z21] are on github [kzc](#) as a part of the paper [Wu et al.](#) which builds on [Zhang et al. \(2021b\)](#).

D.1.1. DISCUSSION OF RESULTS

Comparison with [K19]: from the sample complexity comparison in Table 2, we see that both [K19] and dual-EnKF have similar sample complexity. However, since [K19] is a policy gradient type algorithm, they need to run copies of the LQG system forward in time for each iteration of their algorithm. Since we need to execute only one iteration of the linear dynamical system, it can be expressed as vector matrix multiplications in python, and we use that structure to leverage the vectorization capabilities of numpy to obtain an order of magnitude acceleration in simulation time.

Comparison with [Z21]: from the sample complexity comparison in Table 2, we see that [Z21] has a much higher sample complexity than dual EnKF. it stems from that fact that [Z21] have a policy gradient type approach, which simulates the system forward in time for each iteration. Moreover, [Z21] estimates the finite horizon gain as a function of time, which requires stacking all the gains into one large matrix, that increases the problem size significantly.

D.1.2. MODEL AND SIMULATION PARAMETERS

We run all three algorithms on a discrete time used in [Z21], and plot the simulation time required to reach a specified relative error in gain and cost. We recall that [Z21] considers a finite time LEQG problem with $\theta > 0$ and [K19] considers an infinite horizon LQG problem. Both works are in discrete time, and the details of the dynamical system, the optimal control parameters, and simulation parameters are all below. We convert the discrete time system to a continuous time system for running the dual EnKF (conversion formulas in Appendix D).

The discrete time system has the following parameters (same as the one in (Zhang et al., 2021b, Section 5)):

$$A_d = \begin{bmatrix} 1 & 0 & -5 \\ -1 & 1 & 0 \\ 0 & 0 & 1 \end{bmatrix}, \quad B_d = \begin{bmatrix} 1 & -10 & 0 \\ 0 & 3 & 1 \\ -1 & 0 & 2 \end{bmatrix}, \quad \sigma_d = \begin{bmatrix} 5 & 0 & 0 \\ 0 & 2 & 0 \\ 0 & 0 & 2 \end{bmatrix}$$

$$Q_d = \begin{bmatrix} 1 & 0 & 0 \\ 0 & 1 & 0 \\ 0 & 0 & 1 \end{bmatrix}, \quad \text{and } R_d = \begin{bmatrix} 4 & -1 & 0 \\ -1 & 4 & -2 \\ 0 & -2 & 3 \end{bmatrix}$$

We convert it to continuous time using a first order approximation with a discretization step size $\tau_d = 0.1$ s as follows:

$$A = \frac{\log(A_d)}{\tau_d}, \quad B = \frac{B_d}{\tau_d}, \quad \sigma = \frac{\sigma_d}{\tau_d}$$

$$Q = \frac{Q_d}{\tau_d}, \quad R = \frac{R_d}{\tau_d}, \quad G = Q_d$$

A simulation step size $\tau = 0.002$ s is used in our dual EnKF algorithm and for the finite time LEQG simulation, the risk parameter is set as $\theta = 0.2$ with the simulation time horizon as $T = 0.5$ s, i.e. 5 discrete time steps.

D.1.3. DESCRIPTION OF PROCEDURE

In the Figure 3, the results of the number of particles with $N = 100, 200, 300, \dots, 1000$ in our dual EnKF algorithm are presented. For the algorithm in [K19], iteration steps of 100,000 is used, and the

results of time horizon as 3000, 3500, 4000, 5000, 6000 and 6500 time steps are presented. For the algorithm in [Z21], six linear spacing results of error in cost (and in gain), ranging from min error with 100,000 iteration steps to 10% (and 60%), are presented. All results are averaged over 100 runs to find the expectation and the standard deviation. All the results plotted in Figure 3. The [Z21] and [K19] algorithms are run till a certain error in cost or gain is reached, and the computation time is recorded. The EnKF is always run for 10 second simulation period, and the computation time is recorded. Therefore, we document the computation time required to reach a certain value of error. Since the PO algorithms have random number generators, the computation time needed to achieve a certain error lies in a range of values. The EnKF also has a random number generator hence it also exhibits a range of values, but they are very tightly concentrated around the mean.

All the simulations are executed on a desktop iMac computer equipped with a 3 GHz 6-Core Intel Core i5 processor with python3. The device also has a 32GB 2667MHz DDR4 memory and a Radeon Pro 560X 4GB graphic card. Simulation times were measured in python using the `time.time()` function found in the `time` module.

When analyzing error in gain (ϵ^{gain}), we first recall that for [Z21] and dual EnKF, due to the finite time horizon, both K^{alg} and \bar{K}^{opt} are functions of time, while for [K19] it is only one values, the infinite horizon gain. To compute the error in gain, we first need to find the optimal gain (\bar{K}^{opt}) and the gain output by the algorithm (K^{alg}). For [Z21] and [K19] we use the output directly from the codes provided in the following manner. Both codes solve the Riccati equation and output \bar{K}^{opt} . To find the error, we calculate the relative error between the K^{alg} obtained after each iteration, and \bar{K}^{opt} . For dual EnKF, we find \bar{K}^{opt} by solving the Riccati equation and compare it with the \bar{K}^{alg} from the algorithm. To get an estimate of the infinite horizon gain using the dual EnKF, we simply consider refer to the formula in Section .

To calculate the error in cost (ϵ^{cost}), we need the cost produced by the system when the gain produced by the algorithm is applied to it (c^{alg}), and the cost produced on application of the optimal gain (c^{opt}). For [Z21] and [K19] we use the output directly from the codes provided. The codes calculate both c^{alg} and c^{opt} . For dual EnKF, to find c^{opt} and c^{alg} , we find the cost incurred by applying the optimal infinite horizon gain and estimated infinite horizon gain respectively to the system. Given a gain, the cost incurred is computed by solving a Lyapunov equation Davis (1977) for LQG or running a system forward in time and averaging the cost incurred for LEQG.

The simulation time for EnKF records time needed to execute both Algorithm 1 and 2.

D.2. Path integral control

D.2.1. DISCUSSION OF RESULTS

We observe that dual EnKF provides over an order of magnitude gain in simulation time, even though the path integral approach is a model based approach. In this simulation as well, we leverage python computation speed in performing matrix vector multiplications.

D.2.2. MODEL AND SIMULATION PARAMETERS

We run both algorithms on the spring mass damper system (Appendix E.1). We discretize the system when implementing the MPPI algorithm using a discretization step size of 0.1s. We vary the number of masses in the system to vary the dimension of the state.

D.2.3. DESCRIPTION OF PROCEDURE

In Figure 3, we present a comparative analysis of two algorithms: the dual EnKF algorithm and the MPPI algorithm. Both algorithms were evaluated over a 10-second simulation period, with each configuration tested across 15 independent runs to determine average performance metrics and their standard deviations. Therefore, we document the error achieved and the corresponding computation time achieved by that algorithm. Since both algorithms have random number generators, for the same computation time, there is a range of errors that are achieved.

For the dual EnKF algorithm, we tested four different particle configurations ($N = 100, 500, 1000, \text{ and } 5000$ particles), while the MPPI algorithm was evaluated using four different particle counts (10, 50, 100, and 500 particles).

To assess scalability, we tested both algorithms across three system dimensions corresponding to 5 masses (10-dimensional system), 10 masses (20-dimensional system), and 20 masses (40-dimensional system). For each configuration, we measured two key performance metrics: computation time and cost error. This experimental setup allows us to analyze how both algorithms perform across different particle counts and system dimensions.

All the simulations are executed on a desktop iMac computer equipped with a 3 GHz 6-Core Intel Core i5 processor with python3. The device also has a 32GB 2667MHz DDR4 memory and a Radeon Pro 560X 4GB graphic card. Simulation times were measured in python using the `time.time()` function found in the `time` module.

The simulation time for EnKF records time needed to execute both Algorithm 1 and 2.

Appendix E. Numerical illustration of error formulas (9),(10))

E.1. Spring mass damper model

This system is taken from [Mohammadi et al. \(2019\)](#). Let the number of masses be d_s . The matrices A and B are as follows:

$$A = \begin{bmatrix} 0_{d_s \times d_s} & \mathbb{I}_{d_s} \\ -\mathbb{T} & -\mathbb{T} \end{bmatrix}, \quad B = \begin{bmatrix} 0_{d_s \times d_s} \\ \mathbb{I}_{d_s} \end{bmatrix}$$

then the dimension of the system is $d = 2d_s$, and $\mathbb{T} \in \mathbb{R}^{d_s \times d_s}$ is a Toeplitz matrix with 2 on the main diagonal and -1 on the first sub-diagonal and first super-diagonal. We let C, R, G be identity matrix of suitable dimension. The two values of θ are $\{-0.8, 1.1\}$. For Figure 2 $\sigma = 0.1B, T = 10\text{s}$ and we average MSE data over 500 runs to find the expectation, and for Figure 5 $\sigma = 0.3B, T = 5\text{s}$ and we average energy data over 100 runs to find the expectation. The simulation step size is $\tau = 0.02\text{s}$ for both. For Figure 5 we use 500 particles for all simulations.

We evaluate the control algorithm obtained from the dual EnKF on the spring mass damper system and plot the energy of the system (defined as the norm square of the state). We use 1000 particles, and results are shown over an average of 100 simulations. We see that for as high as 80 dimensions, our algorithm manages to reduce the energy and keep it sufficiently close to zero. Results are found in Figure 5 for the stable and unstable spring mass damper system (where the latter is a mathematical construction obtained by reversing the sign of A to change stability properties of the uncontrolled system).

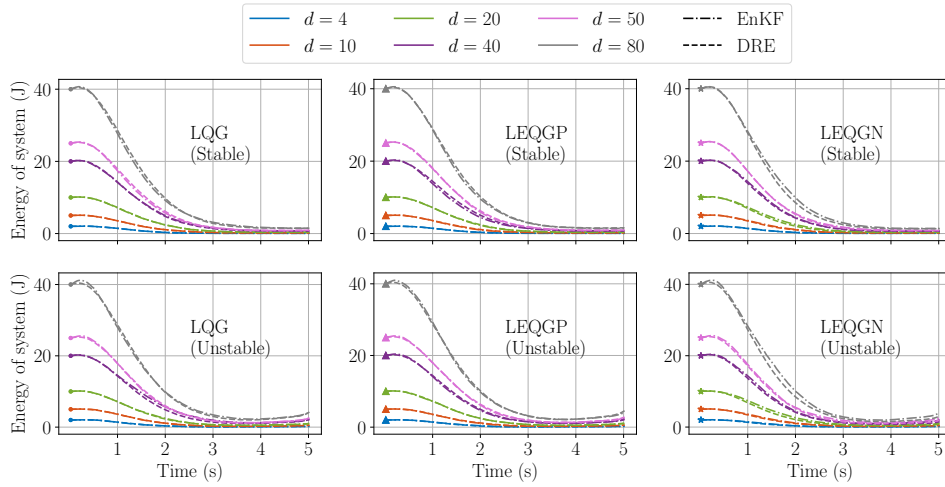


Figure 5: Performance of all three controllers on stable spring mass damper system.

E.2. Random System

We choose a random d -dimensional system is in its controllable canonical form with

$$A = \begin{bmatrix} 0 & 1 & 0 & 0 & \dots & 0 \\ 0 & 0 & 1 & 0 & \dots & 0 \\ \vdots & & & & & \vdots \\ a_1 & a_2 & a_3 & a_4 & \dots & a_d \end{bmatrix}, \quad B = \begin{bmatrix} 0 \\ 0 \\ \vdots \\ 1 \end{bmatrix}$$

where $(a_1, \dots, a_d) \in \mathbb{R}^d$ are i.i.d. samples drawn from $\mathcal{N}(0, 1)$. The matrices C, R, G , are identity matrices of appropriate dimension $\sigma = 0.1B$ and $\theta \in \{1.1, -0.8\}$. For all simulations, $T = 10$, and $\tau = 0.02$, and $N = 500$ particles.

Figure 1 shows the convergence of the 100 entries in $P_t^{(N)}$ to the solution of the ARE. Figure 6 shows the open-loop poles (eigenvalues of the matrix A) and the closed-loop poles (eigenvalues of the matrix $(A + BK_0^{(N)})$). As noted earlier, the closed-loop poles are all stable, whereas some open-loop poles have positive real parts.

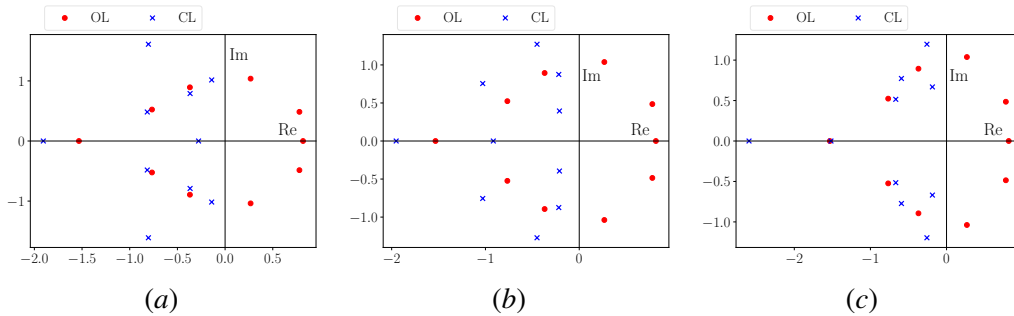


Figure 6: Open and closed-loop poles for (a) LQG (b) LQEG ($\theta > 0$) (c) LEQG ($\theta < 0$).